Seasonal and diurnal variation in CO fluxes from an agricultural bioenergy crop

M. Pihlatie[1,2], Ü. Rannik[1], S. Haapanala[1], O. Peltola[1], N. Shurpali[3], P. J. Martikainen[3], S. Lind[3], N. Hyvönen[3], P. Virkajärvi[4], M. Zahniser[5], I. Mammarella[1]

[1]Department of Physics, University of Helsinki, P.O. Box 48, FI-00014 University of Helsinki
[2]Department of Food and Environmental Sciences, P.O. Box 56, FI-00014 University of Helsinki
[3]Biogeochemistry research group, Department of Environmental and Biological Sciences, University of Eastern Finland, Yliopistoranta 1D-E, PO Box 1627, Kuopio campus, FI-70211 Finland
[4]Natural Resources Institute Finland, Green technology, Halolantie 31 A, FI-71750 Maaninka Finland
[5]Aerodyne Research, Inc. 45 Manning Road Billerica, MA 01821-3976, USA

Correspondence to: M. Pihlatie (mari.pihlatie@helsinki.fi)

Abstract. Carbon monoxide (CO) is an important reactive trace gas in the atmosphere, while its sources and sinks in the biosphere are only poorly understood. Emissions of CO have been reported from a wide range of soil-plant systems. However, soils are generally considered as a sink of CO due to microbial oxidation processes. We measured CO fluxes by micrometeorological eddy covariance method from a bioenergy crop (reed canary grass) in Eastern Finland over April to November 2011. Continuous flux measurements allowed us to assess the seasonal and diurnal variability, and to compare the CO fluxes to simultaneously measured CO_2, N_2O and heat fluxes as well as relevant meteorological, soil and plant variables in order to investigate factors driving the CO exchange.

The reed canary grass crop was a net source of CO from mid-April to mid-June, and a net sink throughout the rest of the measurement period from July to November 2011. CO fluxes had a distinct diurnal pattern with a net CO uptake in the night and an emission during the daytime with a maximum emission at noon. This pattern was most pronounced during the spring and early summer. During this period the most significant relationships were found between daytime CO fluxes and global radiation, net radiation, sensible heat flux, soil heat flux, relative humidity, N_2O flux and net ecosystem exchange. The strong positive correlation between CO fluxes and radiation suggests towards abiotic CO production processes, whereas, the relationship of CO fluxes with net ecosystem exchange indicates towards biotic CO formation during crop growth. The study shows a clear need for detailed process-studies accompanied with continuous flux measurements of CO exchange to improve the understanding of the processes associated with CO exchange.

1 Introduction

Carbon monoxide (CO) is an important reactive trace gas in the atmosphere where it participates in the chemical reactions with hydroxyl radicals (OH), which may lead to the production of the strong greenhouse gas ozone (O_3). The reactions of CO and OH decrease the atmospheric capacity to oxidize atmospheric methane (CH_4), hence indirectly affecting the lifetime of this important greenhouse gas. Although CO itself absorbs only little infrared radiation from the Earth, the cumulative indirect radiative forcing of CO may even be larger than that of a third powerful greenhouse gas nitrous oxide (N_2O) (Myhre et al., 2013). Anthropogenic activities related to burning of fossil fuel and biomass (e.g. forest fires) and photochemical oxidation of CH_4 and non-methane hydrocarbons are the main sources of CO (Duncan et al., 2007), while the reaction with OH is the major sink of CO in the atmosphere (Duncan and Logan, 2008). Soils are globally considered as a sink for CO due to microbial oxidation processes in the soil (Conrad and Seiler, 1982; Potter et al., 1996; Whalen and Reeburgh, 2001; King and Weber, 2007). According to Conrad and Seiler (1980) the soil consumption of CO is a microbial process, it follows first-order kinetics and can take place in both aerobic and anaerobic conditions. In addition to CO consumption, production of CO has been found from a wide range of soils (Moxley and Smith, 1998; Gödde et al., 2000; King, 2000; Varella et al., 2004; Galbally et al., 2010; Bruhn et al., 2013; van Asperen et al., 2015), plant roots (King and Crosby, 2002; King and Hungria, 2002), living and degrading plant material (Tarr et al., 1995; Schade et al., 1999; Derendorp et al., 2011; Lee et al., 2012) and degrading organic matter (Wilks, 1959; Troxler 1972; Conrad and Seiler 1985b). Emissions of CO from water logged soils have often been attributed to anaerobic production of CH_4 (Funk et al., 1994; Varella et al., 2004); however, most often the CO production has been related to abiotic processes such as thermal or UV- or visible light-induced degradation of organic matter or plant material (Conrad and Seiler, 1985b; Tarr et al., 1995; Schade et al., 1999; Derendorp et al., 2011; Lee et al., 2012; van Asperen et al., 2015; Fraser et al., 2015). Photodegradation involves direct and indirect photodegradation of e.g. litter or organic material (King et al., 2012). In the direct photodegradation, a molecule (e.g. lignin) has absorbed radiation and undergoes direct changes such as fragmentation, intramolecular rearrangement or electron transfer from or to the molecular (King et al., 2012). In the indirect photodegradation, certain photosensitizers absorb the incoming radiation and transfer the energy to other molecules such as triplet oxygen, forming reactive intermediates such as singlet oxygen, hydroxyl radical or hydrogen peroxide, which further can change the chemistry of another non-light-absorbing molecule (e.g. cellulose) or part of the same molecule where the photosensitizer resided (King et al., 2012). Thermal degradation is identified as the temperature-dependent degradation of carbon in the absence of radiation and possibly oxygen (Derendorp et al., 2011; Lee et al., 2012; van Asperen et al., 2015), while the separation between CO formation through thermal degradation and photodegradation, is challenging as indirect photodegradation can take place even in the absence of solar

radiation if adequate thermal energy is present (Lee et al., 2012). Photodegradation activity has also been proposed to facilitate microbial degradation through breaking down organic compounds making them easily available for microbial degradation (see King et al. 2012).

Understanding of the biological processes leading to CO release and the importance of these sources in terrestrial ecosystems are poorly understood (Moxley and Smith, 1998; King and Crosby, 2002; Vreman et al., 2011; He and He, 2014). Formation of CO from living green plants under illumination and the presence of oxygen was found already in the late 1950's by Wilks (1959) and Siegel et al. (1962). The proposed processes, however, partly contradict each other as Wilks (1959) proposed that CO formation in green plants is linked to photodegradative activity involving the chlorophyll system, while Siegel et al. (1962) stated that while some oxygen is required, neither light nor chlorophyll are needed for CO is formation from seeds and growing plants. More recently, CO has been found to be formed e.g. in stressed plants (He and He, 2014), in heme oxidation (Engel et al., 1972; Vreman et al., 2011) and aromatic amino acid degradation processes (Hino and Tauchi, 1987), and in lipid peroxidation reactions (Wolff and Bidlack, 1976).

Most of the reported CO flux measurements are either short-term field experiments (e.g. Conrad and Seiler 1985a; Funk et al, 1994; Zepp et al., 1997; Kuhlbusch et al., 1998; Moxley and Smith 1998; Schade et al., 1999; Varella et al., 2004; Bruhn et al., 2013; van Asperen et al., 2015)), or laboratory incubations with specific treatments of the soil or plant material (Tarr et al., 1995; King and Crosby 2002; Lee et al., 2012). Reported CO flux rates in the field studies mostly range between -2 and 2 nmol m^{-2} s^{-1} with a tendency of higher CO uptake from natural and dry soils compared to managed or water-logged soils (Conrad et al., 1988; Khalil et al., 1990; Funk et al., 1994; Zepp et al., 1997; Moxley and Smith, 1998; Schade et al., 1999; King, 2000; King and Hungria, 2002; Varella et al., 2004; Galbally et al., 2010). Also, there is a tendency of south to north gradient with higher CO emissions from tropical and Mediterranean environments compared to boreal and temperate ecosystems (e.g. Zepp et al., 1997; Kuhlbusch et al., 1998; King, 2000; Varella et al., 2004; Galbally et al., 2010; Constant et al., 2008; Bruhn et al., 2013; van Asperen et al., 2015). However, the high variation between CO uptake and emission rates does not allow yet to classify the ecosystem types or climatic regions. Tall tower (Andreae et al., 2015) and airborne measurements have indicated source areas of CO both in the Amazon basin (Harriss et al., 1990; Kirchoff and Marinho, 1990) and in North American tundra (Gosink and Kelly 1979; Ritter et al., 1992; 1994) suggesting a connection between high plant biomass and biological CO forming processes.

To our understanding this is the first study to report long-term and continuous field measurements of CO fluxes (F_{CO}) using micrometeorological eddy covariance (EC) method. We measured F_{CO} above a boreal perennial grassland ecosystem, reed canary grass, over a 7-month snow-free period in 2011 by two parallel laser absorption spectrometers. We compared the F_{CO}

with simultaneously measured fluxes of carbon dioxide (CO_2), nitrous oxide (N_2O), heat and energy as well as relevant soil, plant and meteorological variables. This allowed us to analyze the seasonality and diurnal variability in F_{CO}, and to assess the driving variables of the F_{CO}.

2 Materials and methods

2.1 Measurement site

The measurements were conducted on a mineral agricultural soil cultivated with a perennial reed canary grass (RCG, *Phalaris arundinaceae*, L. cv. Palaton) field located in Eastern Finland (63°9'48.69" N, 27°14'3.29" E). The measurements covered a period from snow-melt to the new snowfall, from April to November 2011. Long-term (reference period 1981-2010) annual mean air temperature in the region is 3.2°C and the annual precipitation is 612 mm (Pirinen et al., 2012). The crop was cultivated in the beginning of June 2009. In 2011, the crop was fertilized in the beginning of the growing season (23 May) with an N-P-K-S fertilizer containing 76 kg N ha^{-1} (NO_3-N : NH_4-N = 47:53). The crop from the previous season was kept at the site over the winter (Burvall, 1997), and was harvested on 28 of April (day 118) (Lind et al., 2016). The spring period (days 118-160) was characterized by fast crop growth with the crop height increasing from about 10 cm in mid-May to 1.7 m in late June, reaching the maximum height of 1.9 m in early July. The field was 6.3 ha in size and from the sampling location of the EC measurement system the footprint was homogenous in all directions, extending 162, 137, 135 and 178 m to N, E, S and W, respectively.

The soil at the site is classified as a Haplic Cambisol/Regosol (Hypereutric, Siltic) (IUSS Working Group WRB, 2007) and the texture of the topsoil (0–28 cm) varied from clay loam to loam based on the US Department of Agriculture (USDA) textural classification system. Soil pH varies from 5.4 to 6.1 within the ploughing layer from the surface to about 30 cm, and soil organic matter content between 3 and 11%. The average C/N ratio in the ploughing layer was 14.9 (ranging from 14.1 to 15.7).

We performed footprint analysis in order to identify the source area of the flux measurements. Two limiting cases were analysed: first, a low crop representing the beginning of the campaign, and second, canopy with 1.9 m height representing the RCG canopy after mid-summer. The measurement heights 2.2 and 2.4 m were used in the analysis, respectively. In the first case we represented the low canopy as the surface with aerodynamic roughness 0.04 m (determined from measurements), in the second case a canopy with leaf area distribution characteristic to RCG crops was represented by a beta

distribution. In both cases the sources were assumed at the soil surface. Such an assumption was made due to limited information on source-sink behaviour (see Sect. 3 below), and also in order to obtain more conservative footprint estimates. Three stability classes representing unstable (the Obukhov length L = -10 m), near-neutral (L = -100 m) and stable (L = +10 m) conditions were considered. The footprint evaluation was performed by using the Lagrangian stochastic trajectory simulations (e.g. Rannik et al., 2003). The upwind distance contributing 80% of the flux was identified for low/high canopy as follows: 53/23 m, 83/34 m, and 166/60 m for unstable, near-neutral, and stable stratifications, respectively. The conducted footprint analysis reveals that the presence of a canopy significantly reduces footprint extent. Note that the conservative footprint scenario with no canopy is applicable only for a short period of time due to fast canopy growth in the beginning of the campaign (see Fig. 1c). Considering that prevailing wind direction during the measurement period was from SE and SSW directions, and the wind direction interval 110-315° contributed 90% of the half-hour periods used in the analysis, the footprint analysis hence confirms that the footprint was sufficient and the measurements well represent the RCG canopy.

2.2   CO flux measurements

The EC measurements were made as a part of the ICOS (Integrated Carbon Observation System) Finland program during April to November 2011. Here we report the results of F_{CO} calculated from the concentration measurements by two continuous-wave quantum cascade lasers: AR-CW-QCL (model CW-TILDAS-CS Aerodyne Research Inc., see e.g. Zahniser et al., 2009) and LGR-CW-QCL (model N2O/CO-23d, Los Gatos Research Inc., see e.g. Provencal et al., 2005). The measurements by AR-CW-QCL extended the whole measurement period from April to November 2011, whereas for LGR-CQ-QCL data is available from later summer to the end of the measurement period (days 206-330). Fluxes by the two analyzers are compared, however, due to the longer data coverage, the diurnal and seasonal variation in F_{CO} is assessed using data from AR-CW-QCL only. The AR-CW-QCL and LGR-CQ-QCL were the same as used in the intercomparison of four laser-based fast-response gas analyzers to measure nitrous oxide (N_2O) fluxes (Rannik et al., 2015).

The measurement height was 2.2 m until 30 June 2011 when the height was raised to 2.4 m due to the growth of RCG. The gas inlets of the closed-path analyzers were located 10 cm below a sonic anemometer (USA-1, Metek Germany GMBH, respectively) used for measuring turbulent wind components. In addition, CO_2 and H_2O fluxes were measured at the site by an infrared gas analyzer (LI7000 – Li-Cor Inc., Lincoln, NE, USA) connected to a sonic anemometer (R3-50, Gill Solent Ltd., UK). The closed-path gas analyzers were located in an air conditioned cabin at about 15 m east from the air inlet and the anemometers. This wind direction (50-110° sector) was therefore discarded from further analysis due to possible disturbances to flux measurements. Sample lines (PTFE) were shielded and heated slightly above ambient air temperature.

5

Sample lines were 16 meters in length, their inner diameters were 4 and 8 mm, the sample air flow rates were 13.2 and 11.6 LPM (Rannik et al., 2015). Based on material testing with LGR-CW-QCL, the PTFE tubing was found inert with respect to CO in a constant-flow setup and flow rate of 2.5 LPM (unpublished data). The EC measurements were sampled at 10 Hz frequency. Further details on the EC set-up, instrument specifications and data acquisition, can be found in Rannik et al.

5 (2015) and Lind et al. (2016).

2.3 Supporting measurements

A weather station located at the site monitored continuously several meteorological and soil parameters such as air temperature (T_{air}) and relative humidity (RH) (model: HMP45C, Vaisala Inc.), precipitation (P_r) (model: 52203, R.M. Young

10 Company), global (R_{glob}) and net radiation (R_{net}) (model: CNR1, Kipp&Zonen B.V.), photosynthetically active radiation (PAR, model: SKP215, Skye instruments Ltd.), soil heat flux at 7.5 cm depth (G) (model: HPF01SC, Hukseflux), soil temperatures at 2.5, 5, 10, 20 and 30 cm depths (T_{soil}) (model: 107, Campbell Scientific Inc.), and soil water content at 2.5, 5, 10 and 30 cm depths (SWC) (model: CS616, Campbell Scientific Inc.). All meteorological data were recorded as 30 min mean values and stored using a datalogger (model: CR 3000, Campbell Scientific Inc.).

15

Leaf area index (LAI) was measured at approximately weekly intervals during the main crop growth period using a plant canopy analyser (model: LAI-2000, LiCor). Green area index (GAI) was estimated on weekly basis from plots adjacent to the LAI measurements according to Wilson et al. (2007) and Lind et al. (2016). The GAI measurements were conducted from three locations (1 x 1 m^2) and within each from three spots (8 x 8 cm^2) by counting a number of green stems (S_n) and

20 green leaves (L_n) per unit area and measuring the green area of leaves (L_a) and stems (L_s). The GAI was calculated as
$$GAI = (S_n S_a) + (L_n L_a) \ .$$

2.4   Data processing and analysis

The EC data processing was performed with post-processing software EddyUH (Mammarella et al., 2016). Filtering to eliminate spikes (Vickers and Mahrt, 1997) was performed according to an approach, where the high frequency EC data

25 were despiked by comparing two adjacent measurements. If the difference between two adjacent concentration measurements of CO was greater than 20 ppb, the following point was replaced with the same value as the previous point.

The spectroscopic correction due to water vapour impact on the absorption line shape was accounted for along with the dilution correction. LGR-CW-QCL automatically corrected the water vapour effect by a built-in module in the LGR data acquisition software. The same spectroscopic correction was applied to AR-CW-QCL after a software update in July 2011. Prior to this software update, the respective dilution and spectroscopic corrections to AR-CW-QCL high-frequency CO mole fraction data were performed during the post-processing phase according to Rannik et al. (2015) with the instrument specific CO spectroscopic coefficient (b=0.28) determined in the field.

Prior to calculating the turbulent fluxes, a 2-D rotation (mean lateral and vertical wind equal to zero) of sonic anemometer wind components was done according to Kaimal and Finnigan (1994) and all variables were linearly detrended. The EC fluxes were calculated as 30 min co-variances between the scalars and vertical wind velocity following commonly accepted procedures (e.g. Aubinet et al., 2000). Time lag between the concentration and vertical wind speed measurements induced by the sampling lines was determined by maximizing the covariance. Due to the larger inner diameter (8 mm) of the sampling line in LGR-CW-QCL, the resulting lag time was 4.2 sec compared to that of 0.91 sec for AR-CW-QCL with the sampling line inner diameter of 4 mm. The final processing was, however, done by fixing the time lag to avoid unphysical variation of lag occurring due to random flux errors. Spectral corrections were applied to account for the low and high frequency attenuation of the covariance. The first order response times of the EC systems were determined to be 0.07 and 0.26 sec for the AR-CW-QCL and LGR-CW-QCL systems, respectively, following the method by Mammarella et al. (2009). This resulted in different flux correction factors mainly due to tube damping: For AR-CW-QCL the 5 and 95 percentile values of flux underestimation were 2.1 and 12.2% and for LGR-CW-QCL 5.7 and 21.4%, respectively. Data quality screening was performed according to Vickers and Mahrt (1997) to ensure exclusion of the system malfunctioning as well as unphysical and/or unusual occasions in measurements. We chose to perform tests on single time series to ensure quality of measurements used in the analysis and did not use the flux stationarity test (Foken and Wichura, 1996) because the CO fluxes are frequently small and respectively with large relative random errors. In such cases the tests based on relative errors are not expected to perform well (e.g. Rannik et al., 2003). After quality screening, 66.0% of the F_{CO} data (AR-CW-QCL) was available, with data coverage of 59.2% during the daytime and 75.9% during the night-time. For details of the data processing and quality screening see Rannik et al. (2015).

To evaluate in detail the seasonal changes in F_{CO} and factors affecting the fluxes the data was divided into six periods (days 110-145 = spring (S), days 146-160 = early summer (ES), days 161-181 = mid-summer (MS), days 205-240 = late summer

(LS), days 241-295 = autumn (A), and days 296-325 = late autumn (LA)). The division into these periods was based on seasonal changes in crop growth and development, or changes in F_{CO} and temperature, while the lengths of the periods were kept as similar in length as possible. Also, F_{CO} were not measured during an instrumental break between days 181 and 204. To compare diurnal changes in the F_{CO}, the data was further divided into daytime (F_{CO_day}) and night-time (F_{CO_night}) data. We used sun elevation angle $h<0$ for night-time and $h>0$ for daytime. Pearson correlations between daytime and night-time half-hour average fluxes and other measured parameters were determined. Data processing was performed with Matlab version R2014a (The MathWorks, Inc., United States) and the statistical testing with IBM SPSS statistics 23 (IBM Corporation, United States).

To evaluate the gross CO flux rates (gross F_{CO}), and the influence of temperature on CO uptake, we calculated the gross F_{CO} in two ways 1) by assuming an equivalent CO uptake during daytime as during night-time (constant uptake), and 2) by taking into account temperature dependency (Q_{10} of 1.8) in CO uptake according to Whalen and Reeburgh (2001). The gross F_{CO}, based on a constant CO uptake, was calculated by subtracting the night-time F_{CO} from the daytime F_{CO} for each six measurement periods (Table 2). The temperature dependent gross F_{CO} was calculated solving the *R2* in the equation

$$Q_{10} = \frac{\left(\frac{R2}{R1}\right)^{10}}{(T2-T1)} \quad ,$$

where Q_{10} is 1.8 (Whalen and Reeburgh, 2001), *R1* is the CO uptake rate during night-time (nmol m^{-2} s^{-1}), and *T2-T1* is the temperature difference between daytime (*T2*) and night-time (*T1*) soil temperature at 2.5 cm depth (ºC), respectively, for each of the six measurement periods (Table 2).

3   Results

3.1   Seasonal variation

The RCG field was a net source of CO from mid-April in the spring to mid-June (days 110-160), after which the site turned to a net sink until the end of the measurement period in November 2011 (days 161-322) (Fig. 1). Cumulative CO flux (cum F_{CO}) curves show that the site was a net sink of CO over the 7-month measurement period. During daytime, the net CO fluxes (F_{CO_day}) were positive during the spring and early summer (days 110-160) and again during late summer (days 205-240). These daytime emissions were highest during the spring (Table 1). Night-time CO fluxes (F_{CO_night}) were negative (CO

uptake) throughout the whole measurement period with a trend of increasing CO consumption towards late autumn (Table 1).

The spring emission period (days 110-145) covered a time (days 110-118) with a standing dry crop from the previous year. The old crop was harvested on 28 of April (day 118), after which the ground consisted mainly of short dead plant material and litter, and a slowly sprouting new RCG. The second emission period in early summer (days 146-160) was characterized by fast growing RCG crop, high and fertilizer-induced N_2O emissions (Shurpali et al., 2016), increasing air and soil temperatures, growing leaf area and increasing NEE (Fig. 1). After the crop had reached its maximum height of 1.9 m in mid-June (around day 160), the site started to act as a net sink of CO, followed by a period of net daytime emissions during late summer in July-August (days 205-240). The autumn was characterized by decreasing F_{CO} and slowly dropping temperatures, decreasing radiation intensity, and decreasing photosynthesis activity of the crop (less negative NEE) (Fig. 1).

Comparison of the two gas analyzers, AR-CW-QCL and LGR-CW-QCL, during the period when both were operational (days 205-325), shows that the measured F_{CO} agree reasonably well (Fig. 1f). A correlation scatter plot of the F_{CO} from LGR-CW-QCL against F_{CO} of AR-CW-QCL results on a correlation coefficient of 0.95 and a slope of 0.96 (data not shown). According to this comparison, LGR-CW-QCL shows slightly (4%) smaller fluxes compared to AR-CW-QCL, however, the difference between the two analyzers is very small, giving us confidence in the use of either of the analyzer in further analysis.

3.2 Diurnal variation

The F_{CO} had a distinct diurnal pattern with a near constant CO uptake in the night-time and an emission during the daytime with maximum emissions at noon (Fig. 2). This pattern was most pronounced during the spring, days 110-145, when the maximum daytime CO emissions reached 2.7 nmol m^{-2} s^{-1} (Fig. 2). The net F_{CO} was positive (emission) during the spring and early summer, after which the night-time uptake dominated making the site as a net sink of CO (Fig. 2, Table 1.). Night-time F_{CO} show a near constant uptake of CO over the whole measurement period (Fig. 2, Table 1.). The gross daytime CO emissions (gross F_{CO}) were estimated in two ways: 1) assuming a constant CO uptake over daytime, and 2) accounting for temperature dependent CO uptake according to Whalen and Reeburgh (2001). The gross F_{CO} show that in the daytime the site emitted CO throughout the whole measurement period with the highest emissions during the spring and late summer (Table 2). During mid-summer and autumn the daytime emissions were markedly smaller, and less than half of the emissions during the spring. The smallest gross F_{CO} were measured in late autumn (Table 2). When the temperature dependency in the

CO uptake was taken into account, using a Q_{10} value of 1.8 (Whalen and Reeburgh, 2001), both the daytime CO uptake (F_{CO} uptake day(Q_{10}, 1.8)), and the daytime emission (gross F_{CO} day(Q_{10}, 1.8)) were almost twice as high as the rates without the temperature correction (Table 2).

The diurnal F_{CO} over the six periods followed closely the daily pattern of R_{glob} (Fig. 3). However, the highest radiation intensity was reached during the early summer (days 146-160), while the maximum F_{CO} were observed during the spring (days 110-145) (Figs. 2 and 3).

Compared to the F_{CO}, the diurnal variation in CO_2 exchange, expressed here as NEE, was very small during the spring (days 110-145) (Fig. 4). A rapid increase in LAI and GAI at around day 150 (Fig. 1d) lead to an increase in CO_2 uptake during daytime, which is seen in a distinct diurnal pattern with high CO_2 uptake (negative NEE) during daytime and a small positive NEE during night-time (Fig. 4). Maximum NEE values were reached during mid-June (days 161-181) after which the NEE slowly decreased and the CO_2 uptake disappeared by mid-October (day 290) (Figs 1 and 4).

During early summer, the fluxes of N_2O followed a similar daily pattern as that of F_{CO} with higher daytime N_2O emissions compared to night-time fluxes (Shurpali et al., 2016). This period of high N_2O emissions (days 143-158) was a direct response to the N-P-K-S fertilizer application on 23 May, and it lasted for about 15 days. After this, an opposite diurnal pattern was observed during which the N_2O emissions were on average 50% higher during the night than during the day (Shurpali et al., 2016).

3.3   Driving factors for CO fluxes

The most pronounced relationships between F_{CO} and other measured scalars were found for the daytime data (sun elevation h>0) during the two emission periods in the spring and early summer (Table 3, Figure 5). Furthermore, the strongest correlations were found during the spring between F_{CO_day} and R_{glob} (r=0.760, p<0.01), R_{net} (r=0.760, p<0.01), H (r=0.729, p<0.01) and G (r=0.575, p<0.01). These positive correlations remained significant but became weaker towards the end of the measurement period (Table 3, Figure 5). Strong negative correlations were found during the spring between F_{CO_day} and RH (r=-0.537, p<0.01), and during the early summer with NEE (r=-0.469, p<0.01), while the correlation between daytime F_{CO} and M_{CO}, F_{N2O} or ecosystem respiration (RESP) were very weak throughout the 7-month measurement period (Table 3). Night-time (h<0) F_{CO} (F_{CO_night}) correlated weakly with F_{N2O} (r=-0.336, p<0.01), H (r=0.315, p<0.01), and LE (r=-0.241, p<0.05) in the spring and with M_{soil} (r=0.308, p<0.01) during early summer. A strong negative correlation was found

10

between F_{CO_night} and F_{N2O} during mid-summer (r=-0.607, p<0.01) and late autumn (r=-0.514, p<0.01), and a positive correlation between F_{CO_night} and LE (r=0.459, p<0.05) during mid-summer (Table 4).

4   Discussion

Based on the 7-month EC flux measurements at the RCG crop, we demonstrate that the EC method is suitable for measuring CO fluxes (F_{CO}) from a perennial agricultural crop. We show that the soil-plant system acted as a net source of CO during the spring and early summer and a net sink of CO over the late summer and autumn, and that the F_{CO} had a clear diurnal pattern with net CO emissions during daytime and net CO uptake during night. This source-sink pattern existed over the whole measurement period with decreasing net emissions towards the end of the autumn. To our knowledge, similar long-term and continuous F_{CO} data series measured by the EC method over any ecosystem type does not exist, and hence this study is unique in bringing new insight to the understanding of short-term diurnal and long-term seasonal F_{CO} dynamics at ecosystem-level. Combining the continuous F_{CO} data with simultaneously measured CO_2, N_2O and energy fluxes as well as meteorological and soil variables allowed us to distinguish driving variables of the F_{CO}, and demonstrate the suitability of the EC method to analyze ecosystem-level CO exchange dynamics. Due to the fact that the EC method measures net fluxes, we cannot directly separate between different processes, such as CO production and consumption. However, based on process understanding and our data, we made an assumption that most of the CO production takes place during daytime and that the night-time CO uptake is due to microbial activity. After these assumptions, we divided the data into daytime and night-time periods in order to analyse seasonal changes in dependencies between F_{CO} and its driving variables.

Cumulative CO fluxes (cum F_{CO}) over the whole measurement period showed that the RCG crop was a net sink of CO. This cum F_{CO} estimation may be biased due to the instrumental break during July (days 181-205), during which we do not have an estimate of the CO fluxes. Also, due to the fact that the data processing removed more daytime values (40.8% removed) compared to night-time data (24.1% removed), the night-time CO uptake is weighing more in the cumulative flux estimation, potentially leading to smaller and more negative net fluxes than estimated based on an equal number of flux data from daytime and night-time. We tested a simple statistical gap-filling method to obtain a balanced number of daytime and night-time data, however, as this gap-filling did not change the interpretation of the results, and as we do not have an appropriate process model to account for uptake and emission processes, we decided not to present these results.

11

Based on the seasonal variation, we could divide the F_{CO} to a distinct emission period and an uptake period. During the "emission" period (days 110-160), the soil-plant system was a strong source of CO during daytime and a small sink during night-time. Furthermore, the emission period was divided into a spring emission period (days 110-145) and an early summer emission period (days 146-160), which differed from each other based on the daytime CO emission rates and relationships with other measured variables such as radiation and NEE. The highest CO emissions were observed soon after the snow melt during the spring in April to early May when the air and soil temperatures were rather low, crop was not yet actively photosynthesizing (low LAI, low NEE), while the radiation intensity was already rather high. As suggested by King (2000), the elevated spring-time CO emissions probably resulted from the degradation of the readily available last year's crop and litter, which has been shown to be a significant source of CO (King, 2000; King et al., 2012; Lee et al., 2012). Decreasing amount of this readily degradable litter also partly explains the decreasing trend in CO emissions during spring and early summer (King, 2000).

In general, the F_{CO} rates from the RCG crop in this study fall into the same range as those reported from different natural and managed ecosystems across the different climatic regions (Table 5). There is a tendency of higher CO emissions from tropical and Mediterranean ecosystems compared to northern and boreal ecosystems. The data comparison also indicates net CO uptake from forest ecosystems (Zepp et al., 1997; King, 2000; Kuhlbusch et al., 1998), CO emissions from savanna and croplands ecosystems (King, 2000; Kisselle et al., 2002; Varella et al., 2004; Galbally et al., 2010), and variation between CO uptake and emission from grassland ecosystems (Constant et al., 2008; Bruhn et al., 2013; van Asperen et al., 2015; Table 5). When comparing daytime fluxes, the mean daytime F_{CO} at the RCG of 0.21 nmol m^{-2} s^{-1} is at the lower end of emissions reported in grasslands or croplands (King, 2000; Bruhn et al., 2013; van Asperen et al., 2015), however, the strong seasonality and higher CO emissions during the spring (0.91 nmol m^{-2} s^{-1}) are very similar to the fluxes measured in tropical pastures and croplands (King, 2000; Varella et al., 2004; Galbally et al., 2010). The overall comparison of reported CO fluxes to our results is challenged by the differences in temporal resolution of the flux measurements as most of the reported studies are conducted during daytime and with biweekly to monthly intervals, hence neglecting possible diurnal and seasonal variation in the fluxes (e.g. King, 2000; Varella et al., 2004; Galbally et al., 2010; van Asperen et al., 2015).

To calculate and annual CO balance of the RCG site, we used a mean F_{CO} over the whole measurement campaign of -0.25 nmol m^{-2} s^{-1} to apply for the missing period of day 326 – day 109 (22 November 2011 - 18 April 2012). This annual cumulative F_{CO} of -111 mg CO m^{-2} yr^{-1} naturally has a high uncertainty due to the missing measurements. However, we expect that the F_{CO} are minimal during the snow-cover period in December-February. Whereas, for the spring period during the snow-melt in March-April, the assumption of small F_{CO} does not necessarily hold as the amount of radiation and

temperature increase and the soil surface is freed from the snow allowing the old previous year's crop residues to decompose. Hence, we expect that the use of the mean F_{CO} from the measurement period probably underestimates the F_{CO} during the early spring period.

Similar to our findings from the emission period, soils from boreal to tropical regions have been found to have a clear diurnal
5   pattern with emissions in the noon and uptake during the night (Conrad and Seiler, 1985a; Schade et al., 1999; Kisselle et al., 2002; Constant et al., 2008; van Asperen et al., 2015). The existing literature suggests that the net CO exchange involves simultaneous production and consumption processes occurring in a variety of soil-plant systems. While the consumption is suggested to be a microbial process in the soil (Conrad and Seiler, 1980), the production of CO has been mostly linked with abiotic photodegradation or thermal degradation of soils, organic matter and vegetation (Conrad and Seiler 1985a; 1985b;
10 Moxley and Smith 1998; Lee et al., 2012; Bruhn et al., 2013; Fraser et al., 2015) or to a minor extent to anaerobic microbial activity in wet soils (Funk et al., 1994). In our study, the net CO uptake during night-time indicates that there is a microbial sink of atmospheric CO. We expect that this CO consumption also exists during daytime, and it may be increased due to temperature dependency of the consumption (King, 2000; Whalen and Reeburgh, 2001). We did not find correlation between daytime or night-time CO concentration (M_{CO}) and F_{CO}, indicating that M_{CO} is not limiting CO consumption at our site. In
15 our site the daytime CO consumption, if existing, is overruled by a simultaneous CO production, creating the strong diurnal pattern in the spring and early summer. Based on the temperature response of CO consumption using Q_{10} of 1.8 (Whalen and Reeburgh, 2001), we estimated that the daytime CO uptake (mean of -1.79 nmol m^{-2} s^{-1}) is over two times that in the night (mean -0.77 nmol m^{-2} s^{-1}) (Tables 1 and 2). When this was taken into account in gross F_{CO} calculation, also daytime CO production was markedly higher compared to the daytime CO production without the temperature corrected CO
20 consumption. In a Mediterranean grassland van Asperen et al. (2015) reported night-time CO uptake up to -1.0 nmol m^{-2} s^{-1} and daytime emissions of around 10 nmol m^{-2} s^{-1} by a flux gradient method, while night-time minimum chamber fluxes were -0.8 nmol m^{-2} s^{-1} and daytime maximum chamber fluxes were up to 3 nmol m^{-2} s^{-1}, both measured over about one month period. Other reported diurnal CO fluxes are mostly over 24-hours only, and hence mainly demonstrate the potential variation in the CO exchange over one day (Zepp et al., 1997; Kisselle et al., 2002; Constant et al., 2008).

25 Strong correlations between daytime F_{CO} and R_{glob} (and other radiation components) especially in the spring and early summer indicate that the direct or indirect effects of radiation drives the CO emissions. During the spring period, the strongest correlations were observed between daytime F_{CO} and solar radiation (R_{glob}, R_n), sensible heat flux and soil heat flux, all indicating a close connection between F_{CO} and radiation and heat transfer. Factors supporting the CO production through abiotic photodegradation and thermal degradation processes include high C to N ratio of the plant material, presence

13

of oxygen, greater solar radiation exposure (no shading), and litter area to mass ratio (Tarr et al., 1995; King et al., 2012; Lee et al., 2012). Related to the C to N ratio of the plant material, a meta-analysis shows that CO formation via photodegradation increases with C to N ratio of the plant material (King et al., 2012). Also, as the plant material in our measurement site has a high C to N ratio (mean ±stdev: 66±6.3), and as this dry plant material was well exposed to radiation in the spring, we expect that the conditions were suitable for CO formation through abiotic degradation processes. Correlation between F_{CO} and soil heat flux (G), and that between F_{CO} and T_{air} indicate that also thermal degradation plays an important role in daytime CO formation. As the correlation between F_{CO} and T_{soil} was poor (at maximum r=0.355), the T_{soil} at the depth of 2.5 cm does not seem to reflect the location of CO formation via thermal degradation. However, a better correlation between F_{CO} and T_{air} indicates that most likely majority of thermal degradation or indirect photodegradation takes place on the soil surface or in (dead) plant material on top of the soil where temperature and degradation processes are directly influenced by radiation. A close look at the diurnal pattern of F_{CO} during the autumn and summer days in Figures 2 and 3 during the time of sunrise or sunset reveals that the F_{CO} starts to increase before the sun rise at around 9 am (late autumn, days 296-325), and the F_{CO} in the afternoon continues to decrease after the sun set at around 20 pm (late summer, days 205-240). These phenomena could be explained by temperature driven CO consumption, which according to soil temperatures should have a minimum soon after sunrise, hence affecting to the diurnal variation of the net F_{CO} (data not shown). If also abiotic thermal degradation is temperature dependent as van Asperen et al. (2015) suggested, we do not expect thermal degradation to be responsible for increased CO production during early morning hours before the sunrise, however, this process may have contributed to the prolonged CO formation after the sunset during late summer. Our data does not allow for deeper process-level interpretation, however, these findings also indicate that direct photodegradation is probably not the sole source of CO at the site, and that also indirect photodegradation, thermal degradation or biological processes may play roles in the CO formation.

Based on understanding of biological CO formation, a negative correlation between F_{CO} and NEE would indicate involvement of a biological component in the CO production. Indeed, the F_{CO} and NEE correlated negatively (r=-0.469) during early summer (days 146-160), which gives support to the CO formation from living and actively photosynthesizing plants. On the other hand, a poor correlations between F_{CO} and ecosystem respiration (RESP) throughout the measurement campaign indicates the microbial and plant respiratory activity does not play an important role in CO formation. At the RCG crop, the early summer CO emission period in May - June (days 146-160) coincides with the steepest slope in CO_2 uptake (more negative NEE), supporting the findings of Bruhn et al. (2013) and Fraser et al. (2015) that CO can be emitted not only from dead plant matter but also from living green leaves. Similarly, we measured daytime CO emissions during July-August (days 205-240) when the crop had reached maximum height and was photosynthesizing actively, and when the dead plant

14

litter on the ground was fully shaded from the sun by up to 1.9 m high crop and maximum LAI of 5.3 m^2 m^{-2}. The fact that the CO emissions during the summer periods were lower than those during the spring are in line with the suggestion that the CO emissions from photodegradation generally decrease with increasing leaf area index (King et al., 2012), and that the CO photoproduction efficiency is lower for living plants compared to senescent or dead vegetation (Tarr et al., 1995; Erickson et al., 2015).

Although we cannot separate between biotic and abiotic CO formation at the bioenergy crop, our findings of daytime net CO emissions also during the peak LAI in July and maximum NEE, indicate that some CO may also be formed via plant physiological processes. In fact, CO has been found to be formed in living green plants under illumination and the presence of oxygen already in the 1950's (Wilks, 1959). Different abiotic stresses seem to induce CO production in plants (He and He, 2014) and biological CO formation has been observed via heme oxidation (Engel et al., 1972; Vreman et al., 2011), aromatic amino acid degradation (Hino and Tauchi, 1987), and lipid peroxidation reactions (Wolff and Bidlack, 1976). Carbon monoxide is also suggested to play an important role in cell-cell signalling (Ingi et al., 1996; He and He, 2014) and regulation of root growth (Xuan et al., 2007; Guo et al., 2008). The importance of these biological CO forming processes to the global CO budget is, however, still remain largely unknown (King and Crosby, 2002). An aspect demonstrating the lack of understanding in sink-source dynamics of CO, King and Crosby (2002) showed that plant roots are capable of producing CO, and that this CO source can be as high as the current global estimate of CO sink by soils.

With respect to F_{N2O} and F_{CO}, we do not expect a strong relationship due to the difficulties in separating between overlapping abiotic CO production, microbial CO consumption (Conrad and Seiler, 1980; Moxley and Smith 1998), and microbial N_2O production/uptake in the soil. Nitrifiers are among a diverse microbial community oxidizing CO in soils (Jones and Morita, 1983; King and Weber, 2007). Hence a high nitrification activity may be reflected in higher CO consumption in the soil. In the field, this could be visible during night-time when the CO consumption is expected to dominate the net CO fluxes, while in most of the year during daytime the CO production overrides the consumption. If a large fraction of the CO uptake was due to nitrification activity, we should be able to see this in negative correlation between night-time F_{N2O} and F_{CO_night}. In fact, we found significant negative correlations between F_{N2O} and $F_{CO:night}$ in the spring (r=-0.336), mid-summer (r=-0.607) and late autumn (r=-0.514). These correlations were significant but much weaker during the daytime (Table 3). These findings hint towards the role of nitrifiers in CO consumption at the reed canary grass site. However, we have no process data from the site showing the link between nitrifiers and CO consumption.

In our study, the fact that the strong correlations during the emission period between F_{CO} and global radiation, sensible heat flux and soil heat flux disappeared during the late summer and autumn indicates that the driving factors for CO exchange

15

during the spring and early summer were different to those during the late-summer and autumn. We expect that when radiation as the driving factor for CO emissions decreased during late summer, soil CO consumption started to dominate, which is seen in the decreasing diurnal cycle in the F_{CO} and also in the strong correlation between F_{CO_night} and F_{N2O}. We also suggest that the source of CO may also have changed from the dead and senescent plant litter in the spring to the green living vegetation during mid-summer. Both of these have been identified as sources of CO via abiotic processes, however, the smaller emissions of CO from the living plants are explained by a lower production efficiency compared to senescent or dead vegetation (Erickson et al., 2015). Still the role of biological CO forming processes remain unresolved and call for further process-studies.

This is the first study to apply EC based techniques to measure long-term variation in F_{CO} at any ecosystem type in the world. In addition to the long-term seasonal variability in the F_{CO}, we were able to identify the driving variables and processes at ecosystem level, findings that have previously been shown with plot scale chamber measurements or in the laboratory. The high diurnal and seasonal variability over the 7-month measurement period shows that there is an urgent need for continuous and long-term assessment of F_{CO}. The limitations of the EC method, such as inability to separate between CO production and consumption processes, naturally increase uncertainties in the interpretation of the results. However, despite these limitations, the data allowed us to distinguish between the daytime and night-time processes involved and to link the diurnal and seasonal variability to abiotic and biotic processes. Also, the EC method has clear advantages over the traditional enclosure methods such as measuring non-disturbed ecosystem fluxes and avoiding surface reactions with measurement material, both supporting the application of the EC method to measure F_{CO} in different ecosystems.

5   Conclusions

Long-term and continuous EC based measurements of F_{CO} over an arable reed canary grass showed clear seasonal variation with net emissions during the spring and early summer, and net uptake of CO during the late summer and autumn. Daytime emissions of CO and night-time uptake of CO demonstrate the dynamic nature of parallel consumption and production processes. Based on daytime and night-time separation of F_{CO}, and correlation analysis between F_{CO} and radiation, T_{soil}, T_{air}, heat fluxes (H, LE), NEE and ecosystem respiration, and F_{N2O} the daytime CO emissions were suggested to be driven mainly by direct and indirect effects of radiation such as heat fluxes and temperature, while the night-time CO uptake was found to be connected to N$_2$O emissions. Although, the measurement approach does not allow to separate between different CO

forming and consuming processes, CO emissions are suggested to mainly result from abiotic photo- and thermal degradation of plant material and soil organic matter whereas the night-time CO uptake was expected to be microbial. This study demonstrates the applicability of the EC method in CO flux measurements at ecosystem scale, and shows the potential in linking the short-term F_{CO} dynamics to its environmental drivers. In order to fully understand the source-sink dynamics and processes of CO exchange, continuous and long-term F_{CO} measurements in combination with process-based studies are urgently needed.

References

Andreae, M. O., Acevedo, O. C., Araùjo, A., Artaxo, P., Barbosa, C. G. G., Barbosa, H. M. J., Brito, J., Carbone, S., Chi, X., Cintra, B. B. L., da Silva, N. F., Dias, N. L., Dias-Júnior, C. Q., Ditas, F., Ditz, R., Godoi, A. F. L., Godoi, R. H. M., Heimann, M., Hoffmann, T., Kesselmeier, J., Könemann, T., Krüger, M. L., Lavric, J. V., Manzi, A. O., Lopes, A. P., Martins, D. L., Mikhailov, E. F., Moran-Zuloaga, D., Nelson, B. W., Nölscher, A. C., Santos Nogueira, D., Piedade, M. T. F., Pöhlker, C., Pöschl, U., Quesada, C. A., Rizzo, L. V., Ro, C.-U., Ruckteschler, N., Sá, L. D. A., de Oliveira Sá, M., Sales, C. B., dos Santos, R. M. N., Saturno, J., Schöngart, J., Sörgel, M., de Souza, C. M., de Souza, R. A. F., Su, H., Targhetta, N., Tóta, J., Trebs, I., Trumbore, S., van Eijck, A., Walter, D., Wang, Z., Weber, B., Williams, J., Winderlich, J., Wittmann, F., Wolff, S., and Yáñez-Serrano, A. M.: The Amazon Tall Tower Observatory (ATTO): overview of pilot measurements on ecosystem ecology, meteorology, trace gases, and aerosols. Atmos. Chem. Phys., 15, 10723–10776, doi:10.5194/acp-15-10723-2015, 2015.

van Asperen, H., Warneke, T., Sabbatini, S., Nicolini, G., Papale, D., and Notholt J.: The role of photo- and thermal degradation for CO_2 and CO fluxes in an arid ecosystem. Biogeosciences, 12, 4161–4174, 2015.

Aubinet, M., Grelle, A., Ibrom, A., Rannik, Ü., Moncrieff, J., Foken, T., Kowalski, A.S., Martin, P.H., Berbigier, P., Bernhofer, Ch., Clement, R., Elbers, J., Granier, A., Grünwald, T., Morgenstern, K., Pilegaard K., Rebmann C., Snijders W., Valentini R. and Vesala, T.: Estimates of the annual net carbon and water exchange of European forests: the EUROFLUX methodology, Advances Ecol, Res., 30, 113-175, 2000.

Bruhn, D., Albert, K. R., Mikkelsen, T. N. and Ambus, P.: UV-induced carbon monoxide emission from living vegetation. Biogeosciences, 10, 7877–7882. doi:10.5194/bg-10-7877-2013, 2013.

Burvall, J.: Influence of harvest time and soil type on fuel quality in reed canary grass (*Phalaris arundinacea* L.), Biomass Bioenerg., 12, 149–154, 1997.

Conrad, R., and Seiler, W.: Role of microorganisms in the consumption and production of atmospheric carbon monoxide by soils. Applied and Environmental Microbiology, 40(3), 437-445, 1980.

Conrad, R., and Seiler, W.: Arid soils as a source of atmospheric carbon monoxide. Geophys. Res. Lett., 9(12), 1353-1356, 1982.

Conrad, R., and Seiler, W.: Influence of temperature, moisture and organic carbon on the flux of H2 and CO between soil and atmosphere. Field studies in subtropical regions. J. Geophys. Res, 90, 5699-5709, 1985a.

Conrad, R., and Seiler, W.: Characteristics of abiological carbon monoxide formation from soil organic matter, humic acids, and phenolic compounds. Environ. Sci. Technol., 19(12), 1165-1169, 1985b.

Constant, P., Poissant, L., and Villemur, R.: Annual hydrogen, carbon monoxide and carbon dioxide concentrations and surface to air exchanges in a rural area (Quebec, Canada). Atmospheric Environ. 42, 5090–5100, 2008.

Derendorp, L., Quist, J.B., Holzinger, R., Röckmann, T.: Emissions of H_2 and CO from leaf litter of *Sequoiadendron giganteum* and their dependence on UV radiation and temperature. Atmospheric Environ., 45, 7520-7524, 2011.

Duncan, B.N., and Logan, J.A.: Model analysis of the factors regulating the trends and variability of carbon monoxide between 1988 and 1997. Atmos. Chem. Phys., 8, 7389-7403, doi:10.5194/acp-8-7389-2008, 2008.

Duncan, B.N., Logan, J.A., Bey, I., Megretskaia, I.A., Yantosca, R.M., Novelli, P.C., Jones, N.B., and Rinsland, C.P.: Global budget of CO, 1988–1997: Source estimates and validation with a global model, J. Geophys. Res., 112, D22301, doi:10.1029/2007jd008459, 2007.

Engel, R.R., Matsen, J.M., Cpahpamn, S.S., and Schwartz, S.: Carbon monoxide production from heme compounds by bacteria. J. Bacteriology, 112(3), 1310-1315, 1972.

Erickson III, D.J., Sulzberger, B., Zepp, R.G. and Austin, A.T.: Effects of stratospheric ozone depletion, solar UV radiation, and climate change on biogeochemical cycling: interactions and feedbacks. Photochem. Photobiol. Sci., 2015, 14, 127-148, 2015.

Fraser, W.T., Blei, E., Fry, S.C., Newman, M.F., Reay, D.S., Smith, K.A., and McLeod, A.R.: Emission of methane, carbon monoxide, carbon dioxide and short-chain hydrocarbons from vegetation foliage under ultraviolet irradiation. Plant, Cell and Environ., 38, 980–989, 2015.

Foken, T. and Wichura, B.: Tools for quality assessment of surface-based flux measurements, Agric. For. Meteorol., 78(1-2), 83–105, doi:10.1016/0168-1923(95)02248-1, 1996.

Gödde, M., Meuser, K., and Conrad, R.: Hydrogen consumption and carbon monoxide production in soils with different properties. Biol. Fertil. Soils, 32, 129-134, 2000.

Guo, K., Xia, K., and Yang, Z-M.: Regulation of tomato lateral root development by carbon monoxide and involvement in auxin and nitric oxide. J. Exp. Bot., 59 (12), 3443-3452, 2008.

He, H., and He. L.: The role of carbon monoxide signaling in the responses of plants to abiotic stresses. Nitric Oxide, 42, 40-43, 2014.

Hino, S., and Tauchi, H.: Production of carbon monoxide from aromatic amino acids by *Morganella morganii*. Archives for Microbiology, 148, 167-171, 1987.

Ingi, T., Cheng, J., and Ronnett, G.V.: Carbon monoxide: an endogenous modulator of the nitric oxide-cyclic GMP signalling system. Neuron, 16, 835-842, 1996.

IUSS Working Group WRB: World Reference Base for Soil Resources 2006, first update 2007, World Soil Resources Reports No.103, FAO, Rome, 128 pp., 2007.

Kaimal, J. C. and Finnigan, J. J.: Atmospheric Boundary Layer Flows. Their Structure and Measurement, Oxford University Press, New York, 1994.

Jones, R.D., Morita, R.Y.: Carbon monoxide oxidation by chemolithotrophic ammonium oxidisers. Can. J. Microbiol. 29, 1545-1551, 1983.

King, G. M.: Impacts of land use on atmospheric carbon monoxide consumption by soils. Global Biogeochem. Cycl., 14, 1161-1172, 2000.

King, G. M., and Crosby, H.: Impacts of plant roots on soil CO cycling and soil-atmosphere CO exchange. Glob. Change Biol., 8, 1085-1093, 2002.

19

King, G. M., and Hungria, M.: Soil-Atmosphere CO Exchanges and Microbial Biogeochemistry of CO Transformations in a Brazilian Agricultural Ecosystem. Applied and Environmental Microbiology, 68(9), 4480-4485, 2002.

King, G. M., and Weber, C. F.: Distribution, diversity and ecology of aerobic CO-oxidizing bacteria. Nature Reviews, Microbiology, 5, 107-118, 2007.

5   King, J.Y., Brandt, L.A., and Adair, E.C.: Shedding light on plant litter decomposition: advances, implications and new directions in understanding the role of photodegradation. Biogeochem., 111, 57-81, 2012.

Kisselle, K. W., Zepp, R. G., Burke, R. A., Pinto, A. S., Bustamante, M. M. C., Opsahl, S., Varella, R. F. and Viana, L. T.: Seasonal soil fluxes of carbon monoxide in burned and unburned Brazilian savannas, J. Geophys. Res., 107(D20), 8051, doi:10.1029/2001JD000638, 2002.

10   Kuhlbusch, T.A.J., Zepp, R.G., Miller, W.L., and Burke, R.A.: Carbon monoxide fluxes of different soil layers in upland Canadian boreal forests. Tellus, 50B, 353-365, 1998.

Lee H., Rahn, T., and Throop, H.: A accounting of C-based trace gas release during abiotic plant litter degradation. Glob. Change Biol., 18, 1185-1195, 2012.

Lind, S.E., Shurpali, N.J., Peltola, O., Mammarella, I., Hyvönen, N., Maljanen, M., Räty, M., Virkajärvi, P., and P. J.
15   Martikainen: Carbon dioxide exchange of a perennial bioenergy crop cultivation on a mineral soil. Biogeosciences, 13, 1255–1268, doi:10.5194/bg-13-1255-2016, 2016.

Mammarella, I., Launiainen, S., Grönholm, T., Keronen, P., Pumpanen, J., Rannik, Ü., and Vesala, T.: Relative Humidity Effect on the High-Frequency Attenuation of Water Vapor Flux Measured by a Closed-Path Eddy Covariance System, J. Atmos. Oceanic Technol., 26, 1856-1866, 2009

20   Mammarella, I., Peltola, O., Nordbo, A., Järvi, L., and Rannik, Ü.: EddyUH: an advanced software package for eddy covariance flux calculation for a wide range of instrumentation and ecosystems, Atmos. Meas. Tech. Discuss., doi:10.5194/amt-2015-323, in review, 2016.

Moxley, J.M., and Smith, K.A.: Carbon monoxide production and emission by some Scottish soils. Tellus, 50B, 151-162, 1998.

25   Myhre, G., D. Shindell, F.-M. Bréon, W. Collins, J. Fuglestvedt, J. Huang, D. Koch, J.-F. Lamarque, D. Lee, B. Mendoza, T. Nakajima, A. Robock, G. Stephens, T. Takemura and H. Zhang.: Anthropogenic and Natural Radiative Forcing. In: Climate Change 2013: The Physical Science Basis. Contribution of Working Group I to the Fifth Assessment Report of the Intergovernmental Panel on Climate Change [Stocker, T.F., D. Qin, G.-K. Plattner, M. Tignor, S.K. Allen, J. Boschung, A.

Nauels, Y. Xia, V. Bex and P.M. Midgley (eds.)]. Cambridge University Press, Cambridge, United Kingdom and New York, NY, USA.

Pirinen, P., Simola, H., Aalto, J., Kaukoranta, J., Karlsson, P., and Ruuhela, R.: Tilastoja Suomen ilmastosta 1981–2010, Finnish Meteorological Institute, Helsinki, 2012.

Potter, C.S., Klooster, S.A., and Chatfield, R.B.: Consumption and production of carbon monoxide in soils: a global model analysis of spatial and seasonal variation. Chemosphere, 33(6), 1175-1193, 1996.

Provencal, R., Gupta, M., Owano, T. G., Baer, D. S., Ricci, K. N., O'Keefe, A., and Podolske, J. R.: Cavity-enhanced quantumcascade laser-based instrument for carbon monoxide measurements, Appl. Optics, 44, 6712–6717, 2005.

Rannik, Ü., Aalto, P., Keronen, P., Vesala, T. and Kulmala, M.: Interpretation of aerosol particle fluxes over a pine forest: Dry deposition and random errors. J. Geophys Res., 108 (D17), AAC 3-1—3-11, 2003. DOI: 10.1029/2003JD003542.

Rannik, Ü., Markkanen, T., Raittila, J., Hari, P., and Vesala, T.: Turbulence statistics inside and over forest: influence on footprint prediction, Boundary-Layer Meteorol., 109(2), 163-189, 2013.

Rannik, Ü., Haapanala, S., Shurpali, N. J., Mammarella, I., Lind, S., Hyvönen, N., Peltola, O., Zahniser, M., Martikainen, P. J., and T. Vesala: Intercomparison of fast response commercial gas analysers for nitrous oxide flux measurements under field conditions. Biogeosciences 12, 415–432, 2015.

Schade, G.W., Hofmann, R.-M., and Crutzen, P.J.: CO emissions from degrading plant matter. Tellus 51B, 889-908, 1999.

Shurpali, N.J., Ü. Rannik, S. Jokinen, S. Lind, C. Biasi, I. Mammarella, O. Peltola, M. Pihlatie, N. Hyvönen, M. Räty, S. Haapanala, M. Zahniser, P. Virkajärvi, T. Vesala and P.J. Martikainen. Diurnal and seasonal variations in nitrous oxide exchange from a perennial bioenergy crop in eastern Finland. Sci. Rep. 6, 25739; doi: 10.1038/srep25739, 2016.

Siegel, S.M., Renwick, G., and Rosen, L.A.: Formation of Carbon Monoxide during Seed Germination and Seedling Growth. Science, 137 (3531), 683-684, 1962.

Tarr, M.A., Miller, W.L., and Zepp, R.G.: Direct carbon monoxide photoproduction from plant matter. J. Geophys. Res., 100, D6, 11403-11413, 1995.

Varella, R.F., Bustamante, M.M.C., Pinto, A.S., Kisselle, K.W., Santos, R.V., Burke, R.A., Zepp, R.G., and Viana, L.T.: Soil fluxes of CO_2, CO, NO and N_2O from an old pasture and from native savanna in Brazil. Ecological Applications, 14(4), Supplement, S221-S231, 2004.

Vickers, D. and Mahrt, L.: Quality control and flux sampling problems for tower and aircraft data, J. Atmos. Ocean. Tech., 14, 512–526, 1997.

21

Vreman, H.J., Wong, R.J., Stevenson, D.K.: Quantitating carbon monoxide production from heme by vascular plant preparations in vitro. Plant Physiol. Biochem., 49, 61-68, 2011.

Wolff, D.G., Bidlack, W.R.: The formation of carbon monoxide during peroxidation of microsomal lipids. Biochemical and Biophysical Research Communications, 2, 15-18, 1976.

Wilks, S.S.: Carbon Monoxide in Green Plants. Science, 129 (3354), 964-966, 1959.

Xuan, W., Huang, L, Li, M., Huang, B., Xu, S., Liu, H., Gao, Y., Shen, W.: Induction of growth elongation in wheat root segments by heme molecules: a regulatory role of carbon monoxide in plants? Plant Growth Regul. 52, 41-51, 2007.

Zahniser, M. S., Nelson, D. D., McManus, J. B., Hern-don, S. C., Wood, E. C., Shorter, J. H., Lee, B. H., Santoni, G. W., Jimenez, R., Daube, B. C., Park, S., Kort, E. A., and Wofsy, S. C.: Infrared QC laser applications to field measurements of atmospheric trace gas sources and sinks in environmental research: enhanced capabilities using continuous wave QCLs, Proc. SPIE, 7222, doi:10.1117/12.815172, 2009.

Zepp, R. G., Miller, W. L., Tarr, M. A., Burke, R. A.: Soil-atmosphere fluxes of carbon monoxide during early stages of postfire succession in upland Canadian boreal forests. J. Geophys. Res. 102(D24), 29301-29311, 1997

Table 1. Mean, median and 25-75th percentiles of the CO fluxes (F_{CO}, nmol m^{-2} s^{-1}) measured in a read canary grass (RCG) crop at Maaninka. Mean daytime (sun elevation, $h_{sun} > 0$) and nighttime ($h_{sun} < 0$) fluxes are calculated during six measurement periods (S = spring, ES = early summer, MS = mid-summer, LS = late summer, A = autumn, LA = late autumn), and over the full measurement period from April to November 2011.

Period, days	F_{CO_day}				F_{CO_night}				net F_{CO}			
	mean	median	25th-75th percentile		mean	median	25th-75th percentile		mean	median	25th-75th percentile	
S, 110-145	0.97	0.68	-0.15	2.00	-0.64	-0.56	-0.97	-0.20	0.41	0.09	-0.57	1.28
ES, 146-160	0.24	0.08	-0.29	0.57	-0.67	-0.49	-0.72	-0.33	0.03	-0.10	-0.45	0.43
MS, 161-181	-0.07	-0.08	-0.40	0.24	-0.67	-0.52	-0.86	-0.22	-0.22	-0.18	-0.55	0.16
LS, 205-240	0.36	0.30	-0.07	0.87	-0.76	-0.49	-0.96	-0.19	-0.09	-0.04	-0.53	0.49
A, 241-295	-0.12	-0.18	-0.48	0.13	-0.66	-0.61	-0.90	-0.32	-0.44	-0.44	-0.77	-0.10
LA, 296-325	-0.62	-0.59	-0.94	-0.26	-1.05	-1.01	-1.37	-0.65	-0.92	-0.89	-1.25	-0.49
All, 110-325	0.21	0.01	-0.41	0.55	-0.77	-0.66	-1.06	-0.33	-0.25	-0.34	-0.79	0.17

Table 2. Mean, median and 25-75th percentiles of the daytime gross CO fluxes (gross F_{CO}, nmol m^{-2} s^{-1}), temperature corrected daytime CO uptake (uptake $F_{CO\ day}$) and temperature corrected daytime gross CO fluxes (gross F_{CO}_day) calculated for the read canary grass (RCG) crop at Maaninka. The flux rates are calculated for six measurement periods (S = spring, ES = early summer, MS = mid-summer, LS = late summer, A = autumn, LA = late autumn), and over the full measurement period (All) from April to November 2011. Soil temperature at 2.5 cm depth is used to correct for the temperature driven CO consumption using Q_{10}-value of 1.8 (Whalen and Reeburgh, 2001). Gross CO fluxes (gross F_{CO_day}) refer to the difference between daytime fluxes (F_{CO_day}) and nighttime fluxes (F_{CO_night}) presented in Table 1.

Period, DOY	gross F_{CO} day				Δt_{soil}	uptake F_{CO} day(Q_{10}, 1.8)				gross F_{CO}_day(Q_{10}, 1.8)			
	mean	median	25th-75th percentile		T_{day}-T_{night}	mean	median	25th-75th percentile		mean	median	25th-75th percentile	
S, 110-145	1.61	1.24	0.83	2.20	2.1	-1.24	-1.09	-1.89	-0.39	2.22	1.76	1.74	2.39
ES, 145-160	0.91	0.57	0.43	0.91	1.2	-1.27	-0.92	-1.36	-0.63	1.51	1.00	1.06	1.20
MS, 160-181	0.59	0.45	0.46	0.46	0.7	-1.23	-0.96	-1.58	-0.41	1.15	0.89	1.18	0.65
LS, 205-240	1.12	0.79	0.89	1.07	0.9	-1.42	-0.91	-1.78	-0.36	1.77	1.21	1.71	1.24
A, 240-295	0.54	0.42	0.41	0.45	1.0	-1.24	-1.13	-1.68	-0.59	1.11	0.95	1.19	0.72
LA, 295-325	0.42	0.42	0.43	0.39	0.3	-1.90	-1.84	-2.49	-1.18	1.28	1.25	1.56	0.92
ALL, 110-325	0.98	0.68	0.65	0.88	3.5	-1.58	-1.37	-2.19	-0.68	1.79	1.38	1.78	1.23

23

Table 3. Pearson correlation matrix for half-hour daytime CO fluxes (F_{CO_day}) during six periods (S = spring, ES = early summer, MS = mid-summer, LS = late summer, A = autumn, LA = late autumn) at the reed canary grass crop in Maaninka. M_{CO} = CO mixing ratio, NEE = net ecosystem exchange, RESP = ecosystem respiration, F_{N2O} = N$_2$O flux, H = sensible heat flux, LE = latent heat flux, T_{air} = air temperature, R_{glob} = global radiation, R_{net} = net radiation, G = soil heat flux, T_{soil} = soil temperature at 2.5 cm, SWC = soil water content at 2.5 cm.

	F_{CO_day} S, 110-145		n	F_{CO_day} ES, 146-160		n	F_{CO_day} MS, 161-180		n	F_{CO_day} LS, 205-240		n	F_{CO_day} A, 241-295		n	F_{CO_day} LA, 296-325		n
M_{CO}	0.080	*	711	0.128	**	510	-0.116	*	436	-0.074		488	0.038		851	-0.284	**	288
NEE	-0.188	**	711	-0.469	**	510	-0.308	**	436	-0.488	**	488	-0.237	**	850	-0.25	**	288
RESP	0.015		711	0.274	**	510	0.272	**	436	0.257	**	488	0.198	**	850	0.077		288
F_{N2O}	-0.219	**	669	0.000		453	-0.293	**	426	-0.026		478	-0.085	*	850	-0.172	**	287
H	0.729	**	711	0.329	**	510	0.234	**	436	0.427	**	488	0.132	**	851	-0.076		288
LE	0.402	**	418	0.398	**	401	0.514	**	224	0.625	**	307	0.317	**	573	0.289	**	185
RH	-0.537	**	711	-0.176	**	510	-0.303	**	436	-0.434	**	488	-0.081	*	851	-0.179	**	288
T_{air}	0.425	**	711	0.344	**	510	0.36	**	436	0.433	**	488	0.241	**	851	0.073		288
R_{glob}	0.760	**	711	0.498	**	510	0.373	**	436	0.549	**	488	0.265	**	851	0.256	**	288
R_{net}	0.760	**	711	0.515	**	510	0.376	**	436	0.558	**	488	0.277	**	851	0.218	**	288
G	0.575	**	711	0.473	**	510	0.406	**	436	0.485	**	488	0.247	**	851	0.033		288
T_{soil}	0.191	**	711	0.282	**	510	0.318	**	436	0.358	**	488	0.206	**	851	0.071		288
M_{soil}	-0.099	**	711	0.033		510	0.095	*	436	0.086		488	-0.105	**	851	0.095		288

**. Correlation is significant at the 0.01 level (2-tailed).

*. Correlation is significant at the 0.05 level (2-tailed).

5

10

15

20

24

Table 4. Pearson correlation matrix for half-hour night-time CO fluxes (F_{CO_night}) during six periods (S = spring, ES = early summer, MS = mid-summer, LS = late summer, A = autumn, LA = late autumn) at the reed canary grass crop in Maaninka. M_{CO} = CO mixing ratio, NEE = net ecosystem exchange, RESP = ecosystem respiration, F_{N2O} = N$_2$O flux, H = sensible heat flux, LE = latent heat flux, T_{air} = air temperature, R_{glob} = global radiation, R_{net} = net radiation, G = soil heat flux, T_{soil} = soil temperature at 2.5 cm, SWC = soil water content at 2.5 cm.

	F_{CO_night} S, 110-145	n	F_{CO_night} ES, 146-160	n	F_{CO_night} MS, 161-180	n	F_{CO_night} LS, 205-240	n	F_{CO_night} A, 241-295	n	F_{CO_night} LA, 296-325	n
M_{CO}	-0.045	380	-0.043	142	-0.279 **	134	-0.165 **	324	-0.110 **	1149	-0.041	700
NEE	0.069	380	-0.167 *	142	-0.118	134	-0.049	324	0.024 **	1149	0.025	700
RESP	0.056	380	0.015	142	-0.006 **	134	0.125 **	324	0.062 *	1149	0.072	700
F_{N2O}	-0.336 **	350	0.034	120	-0.607 **	126	-0.197 **	307	0.009	1140	-0.514 **	696
H	0.315 **	380	0.170 *	142	0.002	134	0.051	324	-0.021 **	1149	0.080 *	700
LE	-0.241 *	74	0.099	72	0.459 *	20	-0.078	62	0.135 **	453	0.161 **	279
RH	0.027	380	-0.016	142	-0.057	134	-0.12 **	324	-0.033	1149	-0.041 **	700
T_{air}	0.107 *	380	-0.013	142	0.092	134	0.249 **	324	0.138 **	1149	0.098 **	700
R_{glob}	0.077	380	0.118	142	-0.096	134	-0.02	324	-0.001	1149	-0.041 **	700
R_{net}	0.011	380	0.111	142	0.026	134	0.087	324	0.043	1149	-0.053 **	700
G	0.050	380	0.029	142	0.121	134	0.207 **	324	0.175 **	1149	0.162 **	700
T_{soil}	0.075	380	-0.146	142	-0.035	134	0.167 **	324	0.038	1149	0.117 **	700
M_{soil}	0.043	380	0.308 **	142	0.212 *	134	0.138 *	324	0.093 **	1149	0.008	700

**. Correlation is significant at the 0.01 level (2-tailed).

*. Correlation is significant at the 0.05 level (2-tailed).

Table 5. Reported CO fluxes measured in the field by chamber (transparent or dark), micrometeorological flux gradient or eddy covariance methods.

Reference	Ecosystem, climate, country	Measurement method	Data period, diurnal cycle	F_{CO} (nmol m^{-2} s^{-1})
Zepp et al., 1997	Black spruce forest, boreal, Manitoba, Canada	Chambers, transparent	3 months, daytime	-1.06
Zepp et al., 1997	Jack pine forest, boreal, Manitoba, Canada	Chambers, transparent	3 months, daytime	-0.58
King, 2000	Pine forest, Northeast, Walpole, Maine, USA	Chambers, dark	1.3 years, daytime	1.12
King, 2000	Mixed hardwood-coniferous forest, Walpole, Maine, USA	Chambers, dark	1.3 years, daytime	0.62
King, 2000	Pine forest, Griffin, Georgia, USA	Chambers, dark	1 year, daytime	-0.21
King, 2000	Pine forest, Tifton, Georgia, USA	Chambers, dark	1 year, daytime	-0.95
Kuhlbusch et al., 1998	Black spruce, boreal, Manitoba, Canada	Chambers, dark	1 year, daytime	-1.11
Galbally et al. 2010	Mallee, Eucalyptus sp. Ecosystem, tropical, Australia	Chambers, transparent	1 year, every 2nd month, daytime	0.61
Kisselle et al., 2002	Cerrado, campo sujo, tropical, Brazil	Chambers, transparent	1 year, monthly, daytime	3.16
Kisselle et al., 2002	Cerrado, stricto sensu, tropical, Brazil	Chambers, transparent	1 year, monthly, daytime	2.66
Varella et al., 2004	Natural cerrado, tropical, Brazil	Chambers, transparent	1.5 years, daytime	1.91
Varella et al., 2004	Pasture (*Brachiaria brizantha*), tropical, Brazil	Chambers, transparent	1.5 years, daytime	1.20
King, 2000	Cropland, corn, Walpole, Maine, USA	Chambers, dark	1.3 years, daytime	2.19
King, 2000	Cropland, sorghum/wheat, Griffin, Georgia, USA	Chambers, dark	1 year, daytime	1.16
King, 2000	Cropland, cotton/peanuts/winter wheat, Tifton, Georgia, USA	Chambers, dark	1 year, daytime	1.03
Galbally et al. 2010	Cropland, wheat, tropical, Australia	Chambers, transparent	1 year, every 2nd month, daytime	0.98
Constant et al., 2008	Grassland, boreal, Quebec, Canada	Flux gradient	1 year, diurnal cycle	-2.11
Bruhn et al., 2013	Grassland, temperate, Denmark	Chambers, dark	2 months, daytime	-0.78
Bruhn et al., 2013	Grassland, temperate, Denmark	Chambers, transparent	2 months, daytime	0.36
van Asperen et al., 2015	Grassland, Mediterranean, Italy	Chambers, transparent	5 weeks, summer, diurnal cycle	0.35
van Asperen et al., 2015	Grassland, Mediterranean, Italy	Flux gradient	1 month, summer, diurnal cycle	1.74
this study	Grassland, reed canary grass, boreal, Finland	Eddy covariance	7 months diurnal cycle	-0.25

Figure captions

Figure 1. (a) Daily mean air and soil temperatures, (b) global radiation sum (R_{glob}), (c) daily precipitation sum (Pr) and soil water content (SWC), (d) weekly leaf area index (LAI) (blue) and green area index (GAI) (green), (e) net ecosystem exchange (NEE), and (f) cumulative CO fluxes (cum F_{CO}; blue and green) and daytime mean CO fluxes (F_{CO_day}; red) over
5   the 9-month measurement period in a reed canary grass crop. Measurement periods (S = spring, ES = early summer, MS = mid-summer, LS = late summer, A = autumn, LA = late autumn) are separated by solid lines.

Figure 2. Diurnal cycle of half-hour average CO fluxes (F_{CO}, nmol m^{-2} s^{-1}) from the reed canary grass crop from six distinct periods during the April to November 2011 measurement campaign. The vertical bars indicate ± 1 standard deviation of the
10   fluxes.

Figure 3. Diurnal cycle of half-hour average global radiation (R_{glob}, W m^{-2}) the reed canary grass crop from six distinct periods during the April to November 2011 measurement campaign. The vertical bars indicate ± 1 standard deviation of the fluxes.

15

Figure 4. Diurnal cycle of half-hour average net ecosystem exchange (NEE, µmol m^{-2} s^{-1}) from the reed canary grass crop from six distinct periods during the April to November 2011 measurement campaign. The vertical bars indicate ± 1 standard deviation of the fluxes.

20   Figure 5. Daytime half-hour average CO fluxes (F_{CO}) against global radiation (R_{glob}), sensible heat flux (H) and net ecosystem exchange (NEE) measured over two emission periods (Spring, 110-145, Early Summer, 146-160) at the reed canary grass crop in Maaninka. The bin averages with ± 1 standard deviation are presented in black.
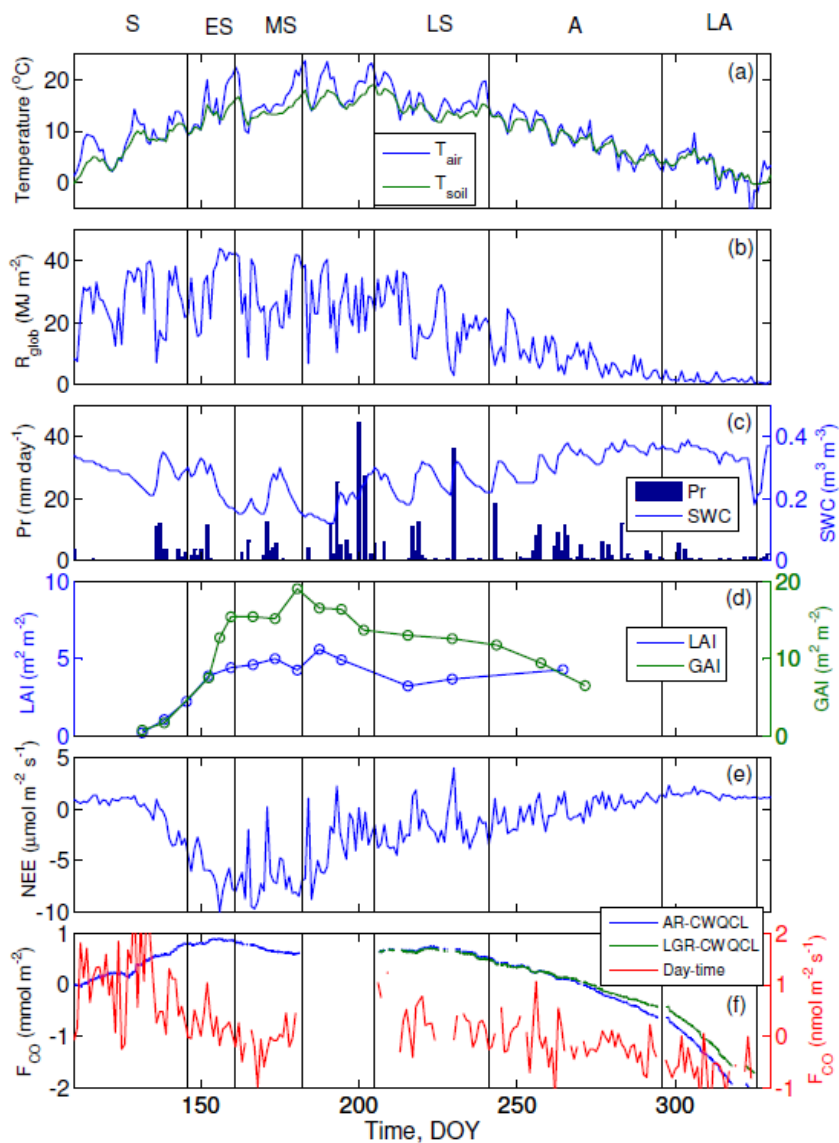
25

Figure 1. (a) Daily mean air and soil temperatures, (b) global radiation sum (R_{glob}), (c) daily precipitation sum (Pr) and soil water content (SWC), (d) weekly leaf area index (LAI) (blue) and green area index (GAI) (green), (e) net ecosystem exchange (NEE), and (f) cumulative CO fluxes (cum F_{CO}; blue and green) and daytime mean CO fluxes (F_{CO_day}; red) over the 9-month measurement period in a reed canary grass crop. Measurement periods (S = spring, ES = early summer, MS = mid-summer, LS = late summer, A = autumn, LA = late autumn) are separated by solid lines.
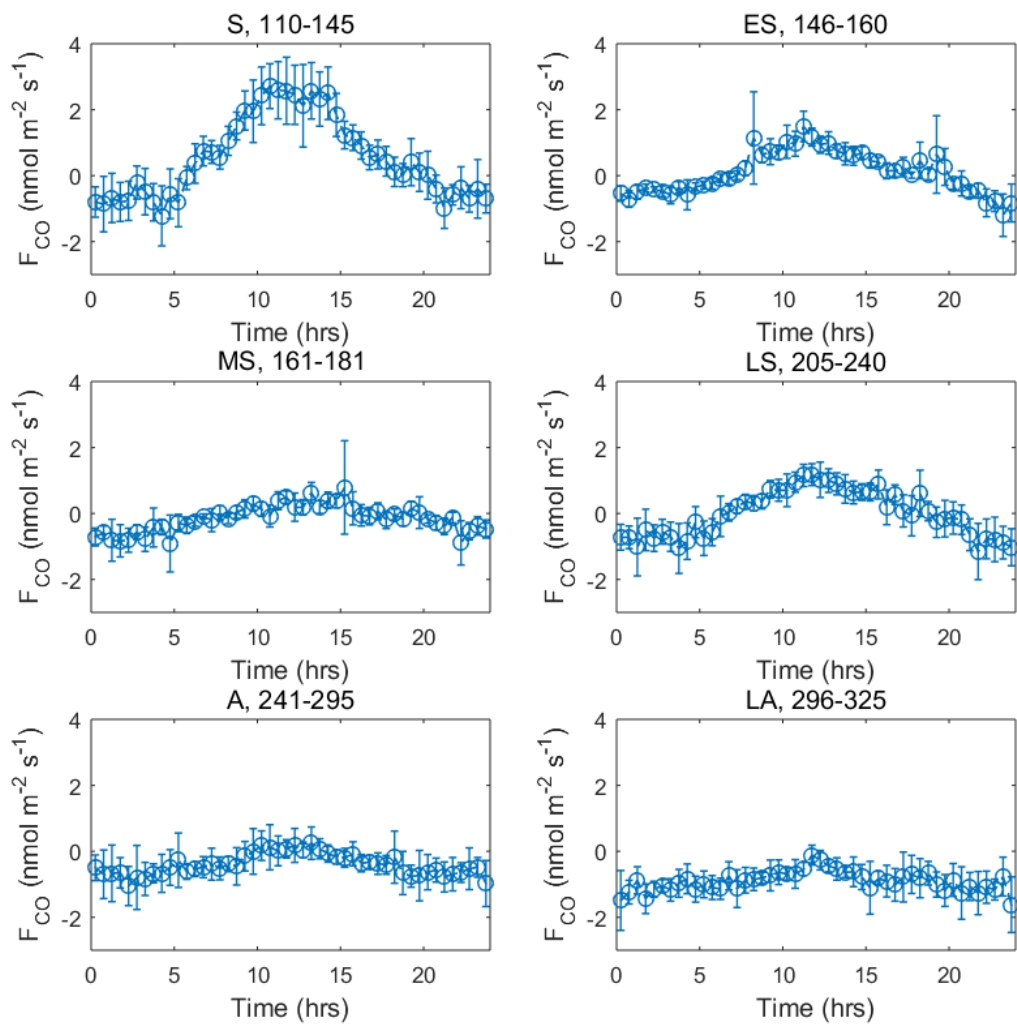
Figure 2. Diurnal cycle of half-hour average CO fluxes (F_{CO}, nmol m^{-2} s^{-1}) from the reed canary grass crop from six distinct periods during the April to November 2011 measurement campaign. The vertical bars indicate ±1 standard deviation of the fluxes.
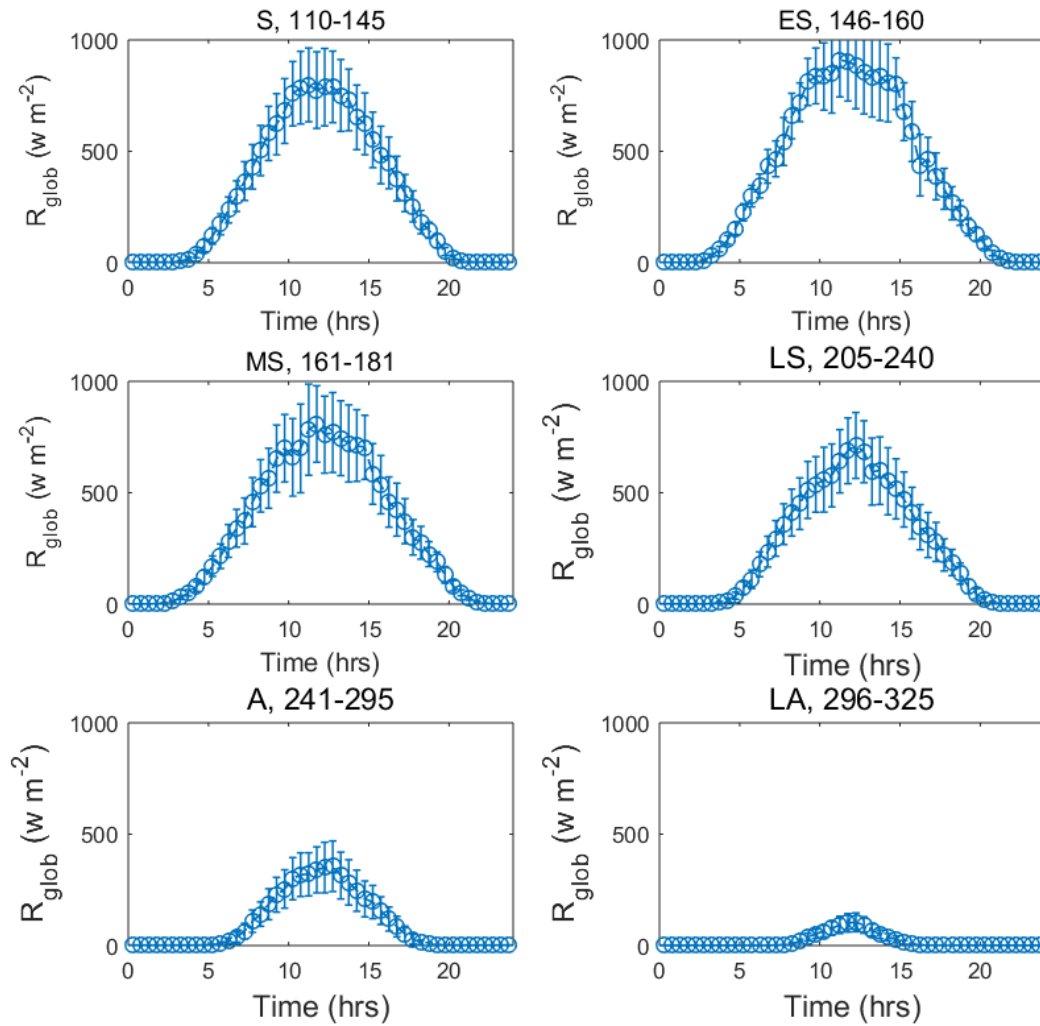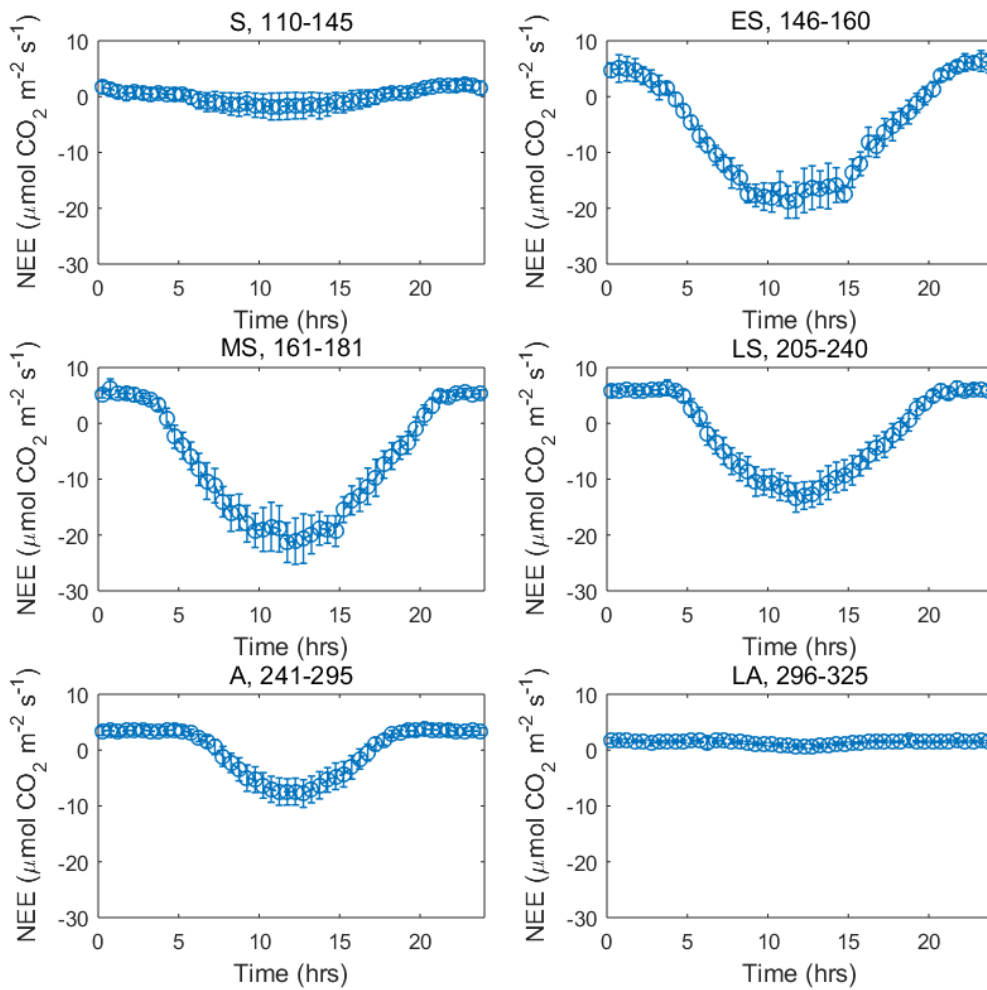
Figure 3. Diurnal cycle of half-hour average global radiation (R_{glob}, W m^{-2}) the reed canary grass crop from six distinct periods during the April to November 2011 measurement campaign. The vertical bars indicate ±1 standard deviation of the fluxes.

Figure 4. Diurnal cycle of half-hour average net ecosystem exchange (NEE, µmol CO_2 m^{-2} s^{-1}) from the reed canary grass crop from six distinct periods during the April to November 2011 measurement campaign. The vertical bars indicate ±1 standard deviation of the fluxes.
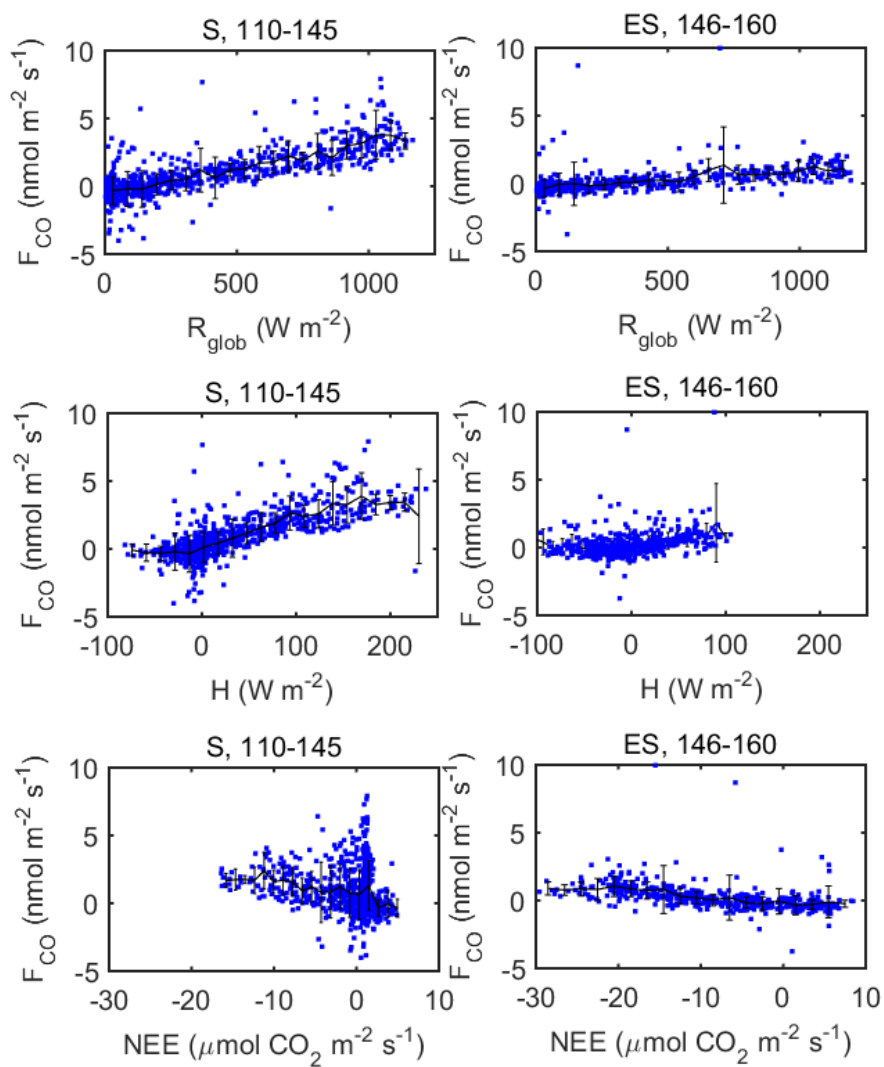
Figure 5. Daytime half-hour average CO fluxes (F_{CO}) against global radiation (R_{glob}), sensible heat flux (H) and net ecosystem exchange (NEE) measured over two emission periods (Spring, days 110-145, Early Summer, days 146-160) at the reed canary grass crop in Maaninka. The bin averages with ±1 standard deviation are presented in black.